Crystal Structure of 3-Carboxy-*cis*,*cis*-muconate Lactonizing Enzyme from *Pseudomonas putida*, a Fumarase Class II Type Cycloisomerase: Enzyme Evolution in Parallel Pathways†

Jian Yang,[‡,§,||] Yi Wang,[‡,§,⊥] Elisa M. Woolridge,[‡] Vandana Arora,[‡] Gregory A. Petsko,[‡,@] John W. Kozarich,[#] and Dagmar Ringe*[,‡,@]

Rosenstiel Basic Medical Sciences Research Center and Departments of Biochemistry and Chemistry, Brandeis University, 415 South Street, Waltham, Massachusetts 02454, and Activx Biosciences, 11025 North Torrey Pines Road, La Jolla, California 92037

Received December 8, 2003; Revised Manuscript Received April 26, 2004

ABSTRACT: 3-Carboxy-*cis*,*cis*-muconate lactonizing enzymes (CMLEs), the key enzymes in the protocatechuate branch of the β-ketoadipate pathway in microorganisms, catalyze the conversion of 3-carboxy-*cis*,*cis*-muconate to muconolactones. We have determined the crystal structure of the prokaryotic *Pseudomonas putida* CMLE (*Pp*CMLE) at 2.6 Å resolution. *Pp*CMLE is a homotetramer and belongs to the fumarase class II superfamily. The active site of *Pp*CMLE is formed largely by three regions, which are moderately conserved in the fumarase class II superfamily, from three respective monomers. It has been proposed that residue His141, which is highly conserved in all fumarase class II enzymes and forms a charge relay with residue Glu275 (both His141 and Glu275 are in adenylosuccinate lyase numbering), acts as the general base in most fumarase class II superfamily members. However, this charge relay pair is broken in *Pp*CMLE. The residues corresponding to His141 and Glu275 are Trp153 and Ala289, respectively, in *Pp*CMLE. The structures of prokaryotic MLEs and that of CMLE from the eukaryotic *Neurospora crassa* are completely different from that of *Pp*CMLE, indicating MLEs and CMLEs, as well as the prokaryotic and eukaryotic CMLEs, evolved from distinct ancestors, although they catalyze similar reactions. The structural differences may be related to recognition by substrates and to differences in the mechanistic pathways by which these enzymes catalyze their respective reactions.

The β-ketoadipate pathway, consisting of a cascade of chromosomally encoded enzymes, catalyzes the catabolism of aromatic compounds into intermediates of the citric acid cycle in both prokaryotic and eukaryotic microorganisms (Figure 1). The pathway has two parallel branches, catechol and protocatechuate (*1*−*4*). The lactonization of *cis*,*cis*-muconates, which is an important step in the pathway, is catalyzed by *cis*,*cis*-muconate lactonizing enzyme (MLE) in the catechol branch and 3-carboxy-*cis*,*cis*-muconate lactonizing enzyme (CMLE) in the protocatechuate branch. MLEs and eukaryotic CMLEs catalyze the lactonization reaction by a *syn*-1,2-addition−elimination reaction, whereas the prokaryotic CMLEs catalyze this cyclization using an *anti*-1,2-addition−elimination reaction (*3*). MLEs represented by *Pseudomonas putida* MLE (*Pp*MLE)[1] convert *cis*,*cis*-muconate into (*R*)-muconolactone. The reaction is reversible and requires the divalent cation Mn^{2+} as a cofactor. The eukaryotic CMLEs such as *Neurospora crassa* CMLE (*Nc*CMLE) convert 3-carboxy-*cis*,*cis*-muconate (3-CM) into 3-carboxy-(*R*)-muconolactone. For prokaryoric CMLEs such as *P. putida* CMLE (*Pp*CMLE), the lactonization product is 4-carboxy-(*S*)-muconolactone. Neither prokaryotic CMLE nor eukaryotic CMLE requires any metal cofactors for catalytic activity. To understand how these reactions are catalyzed, the three-dimensional structures of the relevant enzymes are required. Of these, the structures of *Pp*MLE and *Nc*CMLE are known, while that of *Pp*CMLE, until now, was not.

Our current study and studies from other groups (*3*, *5*−*7*) have shown that both *syn*-cycloisomerases represented by *Pp*MLE and *Nc*CMLE and *anti*-cycloisomerases typified by *Pp*CMLE catalyze their respective cyclization reactions stepwise (Figure 2). The lactonization reaction catalyzed by *syn*-cycloisomerases requires both a general acid and a general base and includes an enol transition state. However,

† This work was supported by NIH Grants GM 32415 and GM40570 to G.A.P. and D.R.

* To whom correspondence should be addressed.

‡ Rosenstiel Basic Medical Sciences Research Center, Brandeis University.

§ These authors contributed equally to this work.

|| Current address: College of Pharmacy and Nutrition, University of Saskatchewan, 110 Science Place, Saskatoon, Saskatchewan, Canada S7N 5C9.

⊥ Current address: Incyte Corp., 100 Cummings Center, Suite 420B, Beverly, MA 01915.

@ Departments of Biochemistry and Chemistry, Brandeis University.

Activx Biosciences.

[1] Abbreviations: *Pp*CMLE, *P. putida* 3-carboxy-*cis*,*cis*-muconate lactonizing enzyme; *Nc*CMLE, *N. crassa* 3-carboxy-*cis*,*cis*-muconate lactonizing enzyme; *Pp*MLE, *P. putida* muconate lactonizing enzyme; 3-CM, 3-carboxy-*cis*,*cis*-muconate; ADSL, adenylosuccinate lyase; ARSL, argininosuccinate lyase; NaP_i, sodium phosphate buffer; DTT, dithiothreitol; IPTG, isopropyl β-D-thiogalactopyranoside; PMSF, phenylmethanesulfonyl fluoride.

10.1021/bi036205c CCC: $27.50
Published on Web 07/22/2004

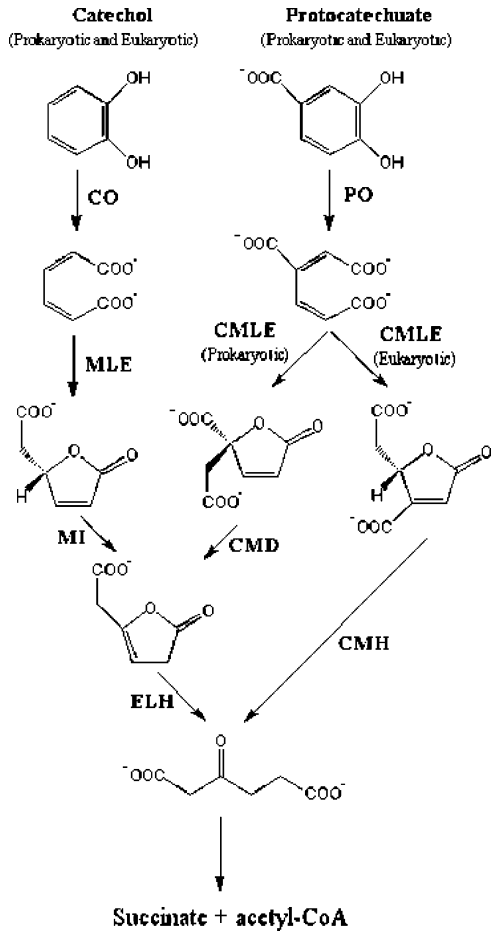

FIGURE 1: β-Ketoadipate pathway in prokaryotic and eukaryotic microorganisms. The pathway consists of two branches. The catechol branch is identical, but the protocatechuate branch is distinct between prokaryotic and eukaryotic microorganisms. The enzymes in the β-ketoadipate pathway include CO (catechol 1,2-dioxygenase), PO (protocatechuate 3,4-dioxygenase), MLE (*cis,cis*-muconate lactonizing enzyme), CMLE (3-carboxy-*cis,cis*-muconate lactonizing enzyme), MI (muconolactone isomerase), CMD (4-carboxymuconolactone decarboxylase), ELH (enol lactone hydrolase), and CMH (3-carboxymuconolactone hydrolase).

the lactonization reaction catalyzed by *anti*-cycloisomerases requires only a general base, and the intermediate has been suggested to be an aci-carboxylate. The lactonizing enzymes, including both MLEs and CMLEs, are members of one of the few groups of enzymes identified so far that are evolved from distinct paths to carry out similar catalytic reactions. Therefore, this group of enzymes becomes an ideal example for studying the functional convergence of enzymes in parallel metabolic pathways.

On the basis of structural observations of enzymes in the mandelate pathway, it has been proposed (*9*) that new enzymes would most often evolve from old ones by the recruitment of the core chemical step, rather than by recruitment of binding specificity for one or more substrates. As a consequence, consecutive enzymes in metabolic pathways would, in general, not resemble each other structurally or in active site arrangement, but rather resemble other enzymes that catalyzed the same fundamental chemical process. For instance, the crystal structure of *P. putida* MLE (*Pp*MLE) shows that each subunit contains a triose phosphate isomerase (TIM) barrel motif as the catalytic domain (*7*, *10*, *11*). Structural and sequence comparisons indicate that both the overall chain fold and the arrangement of the catalytic groups in the active site of *Pp*MLE are remarkably similar to those of mandelate racemase and enolase. Mechanistic similarities of the catalyzed reaction indicate that *Pp*MLE belongs to the enolase superfamily, and it has been suggested that *Pp*MLE and mandelate racemase evolved from the same common ancestor (*9*, *11*, *12*). Subsequent studies in other laboratories (*13*, *14*) have confirmed that this model is indeed valid for the evolution of new enzyme activities, although recruitment of substrate specificity can also occur, as in the case of several enzymes in the trytophan and fatty acid biosynthetic pathways (*15*−*17*).

Parallel pathways present a special problem, however, because they most often involve two varying forms of the substrate, as in the case of the catechol and protocatechuate branches of the β-ketoadipate pathway. In parallel pathways, the enzymatic steps are similar or identical, and the substrates usually resemble each other sufficiently that it is difficult to imagine how recruitment of core chemistry could occur without cross inhibition or breakdown of specificity and independent regulation for each branch.

The muconate lactonizing enzymes provide a unique opportunity to explore this problem. Thus, the eukaryotic *Nc*CMLE has also been shown to catalyze the lactonization reaction via a *syn*-1,2-addition−elimination mechanism. Sequence comparison shows no similarity with MLE, mandelate racemase, or enolase. The crystal structure of *Nc*CMLE shows that it has a typical seven-bladed β-propeller fold with almost ideal 7-fold symmetry (*8*). The active site of *Nc*CMLE is confined within each subunit and located on the top of the central 7-fold pseudosymmetry axis of the β-propeller. To date, there is no evidence showing any allostery among the four active sites of *Nc*CMLE. Nevertheless, from molecular modeling studies, *Nc*CMLE and *Pp*MLE were proposed to recognize their respective substrates using similar residues (*8*). In addition, a hydrophobic pocket at the active site was found in both enzymes, formed by residues Tyr115 and Phe114 in *Nc*CMLE and by residues Ile54 and Tyr59 in *Pp*MLE (*7*, *8*). These similarities, despite the completely different protein scaffolds, argue for convergent evolution to a common chemical mechanism for catalyzing the lactonization of their substrates by both MLEs and eukaryotic CMLEs.

In contrast, the prokaryotic *Pp*CMLE, first purified by Ainsworth and Kirby (*18*), catalyzes cyclization by an anti mechanism, to produce a product with a relative configuration that is the opposite of that of *Pp*MLE at the attacked carbon atom. Sequence analysis and kinetic studies confirmed that *Pp*CMLE belongs to the fumarase class II superfamily, a group of homotetrameric enzymes capable of catalyzing 1,2-addition−elimination reactions (*3*). Three-dimensional structures of a number of members of this superfamily have been determined, including fumarase C (*19*−*21*), adenylosuccinate lyase (ADSL; *22*−*24*), argininosuccinate lyase (ARSL; *25*−*27*), δ-crystallin (*28*−*31*), and aspartase (*32*, *33*). This superfamily of enzymes shares only 20−30% sequence identity, distributed mainly in three moderately conserved regions (Figures 3 and 4A). There are four active sites in the tetrameric molecules of these enzymes, and each active site is formed mainly by three sequence-conserved regions, each contributed by a different monomer subunit (*34*). A highly conserved residue, His141 (ADSL numbering;

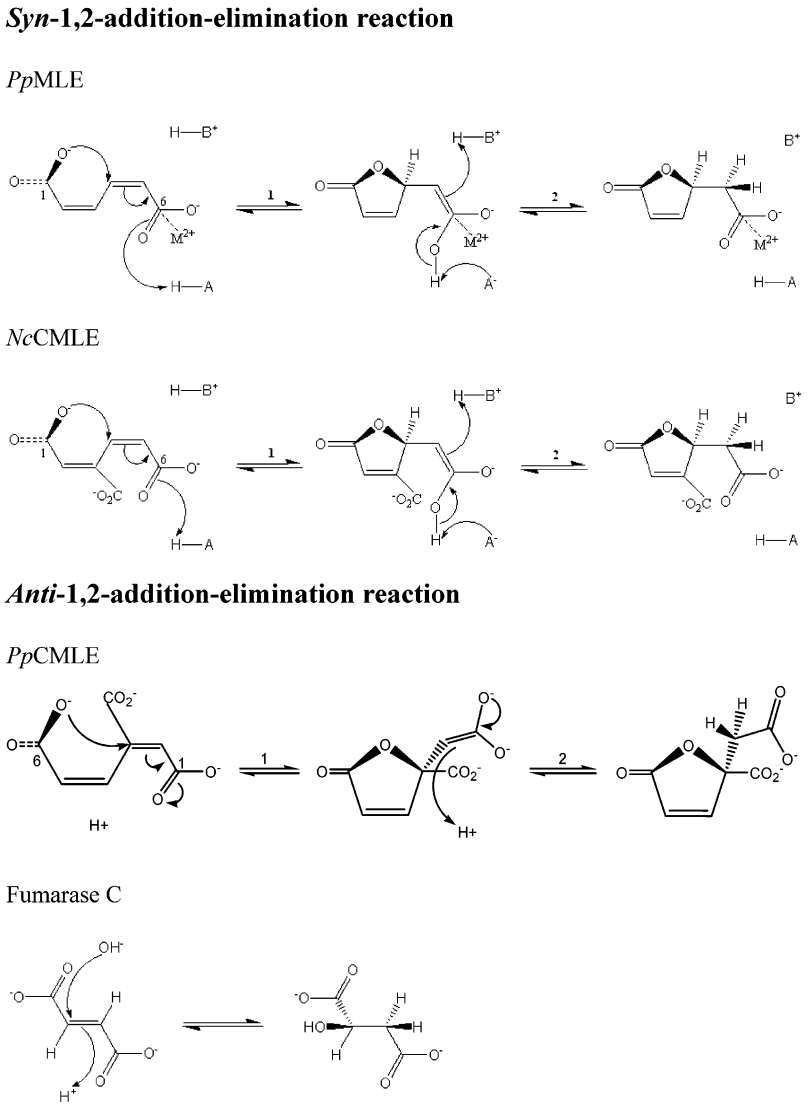

FIGURE 2: Comparison of the catalytic mechanisms for *syn*- and *anti*-1,2-addition−elimination reactions. The enzymes that catalyze *syn*-1,2-addition−elimination reactions are represented by *P. putida* MLE (*Pp*MLE) and *N. crassa* CMLE (*Nc*CMLE). The enzymes that catalyze *anti*-1,2-addition−elimination reactions are typified by *P. putida* CMLE (*Pp*CMLE) and fumarase C.

	Region 1		Region 2		Region 3	
	100	108	150	160	275	289
			*			*
***Pp*CMLE**	VHLG------ATSQD		GRTWLQHATPV		GSSTMPHKRNPVGAA	
***Pa*ADSL**	VHYG------ATSND		GRTHGQWAEPI		GSSAMPHKANPTASE	
Fumarase C	VHPNDDVNKSQSSND		GRTHLQDATPL		GSSIMPGKVNPTQCE	
hARSL	LHTG------RSRND		GYTHLQRAQPI		GSSLMPQKKNPDSLE	
Crystallin	LHTG------RSRND		GYTHLQKAQPI		GSSLMPQKKNPDSLE	
Aspartase	ISPNSHVNSMQSTND		GRTHLQDAVPI		GSSIMPGKVNPVMPE	

FIGURE 3: Sequence alignment of the three moderately conserved regions for *P. putida* CMLE (*Pp*CMLE), *Py. aerophilum* adenylosuccinate lyase (*Pa*ADSL), yeast fumarase C, human argininosuccinate lyase (hARSL), duck δ2-crystallin, and *Bacillus* sp. YM55-1 aspartase in the fumarase class II superfamily. The identical and homologous residues are shown in red and green, respectively. The active sites are composed by these regions from different monomers. The charge relay pair residues (His141 and Glu275 in *Pa*ADSL numbering) are labeled with asterisks. This charge relay pair is broken in *Pp*CMLE. The residues corresponding to this charge relay pair are Trp153 and Ala289, respectively, in *Pp*CMLE (labeled in blue).

His188 in the fumarase numbering) in conserved region 2, forming a charge relay pair with another highly conserved residue, Glu275 (ADSL numbering) in conserved region 3, was identified as the general base in the catalysis by these fumarase class II superfamily members (*24*). However, this charge relay pair is absent in *Pp*CMLE, the residues corresponding to His141 and Glu275 being Trp153 and Ala289 in *Pp*CMLE, respectively (Figures 3 and 4A). Pairwise sequence alignment showed that ADSL is the closest relative of *Pp*CMLE in the superfamily (28.5% identical). However, adenylosuccinate is not a substrate for *Pp*CMLE, and 3-CM is a poor substrate for ADSL (*3*). These observations suggest that significant differences might exist at the active sites between *Pp*CMLE and other superfamily members. Nevertheless, an understanding of the similarities and differences between family members relates not only to the mechanism by which the reaction is catalyzed but also to key motifs of the substrate and the enzyme that are the evolutionarily conserved elements that distinguish the relationship between CMLE and the other members of the fumarase family of enzymes.

Here, we report the 2.6 Å resolution crystal structure of *Pp*CMLE. *Pp*CMLE is the last unique member of the family of muconate lactonizing enzymes as well as the latest in the fumarase class II superfamily whose structure has been determined. This study provides a view of molecular

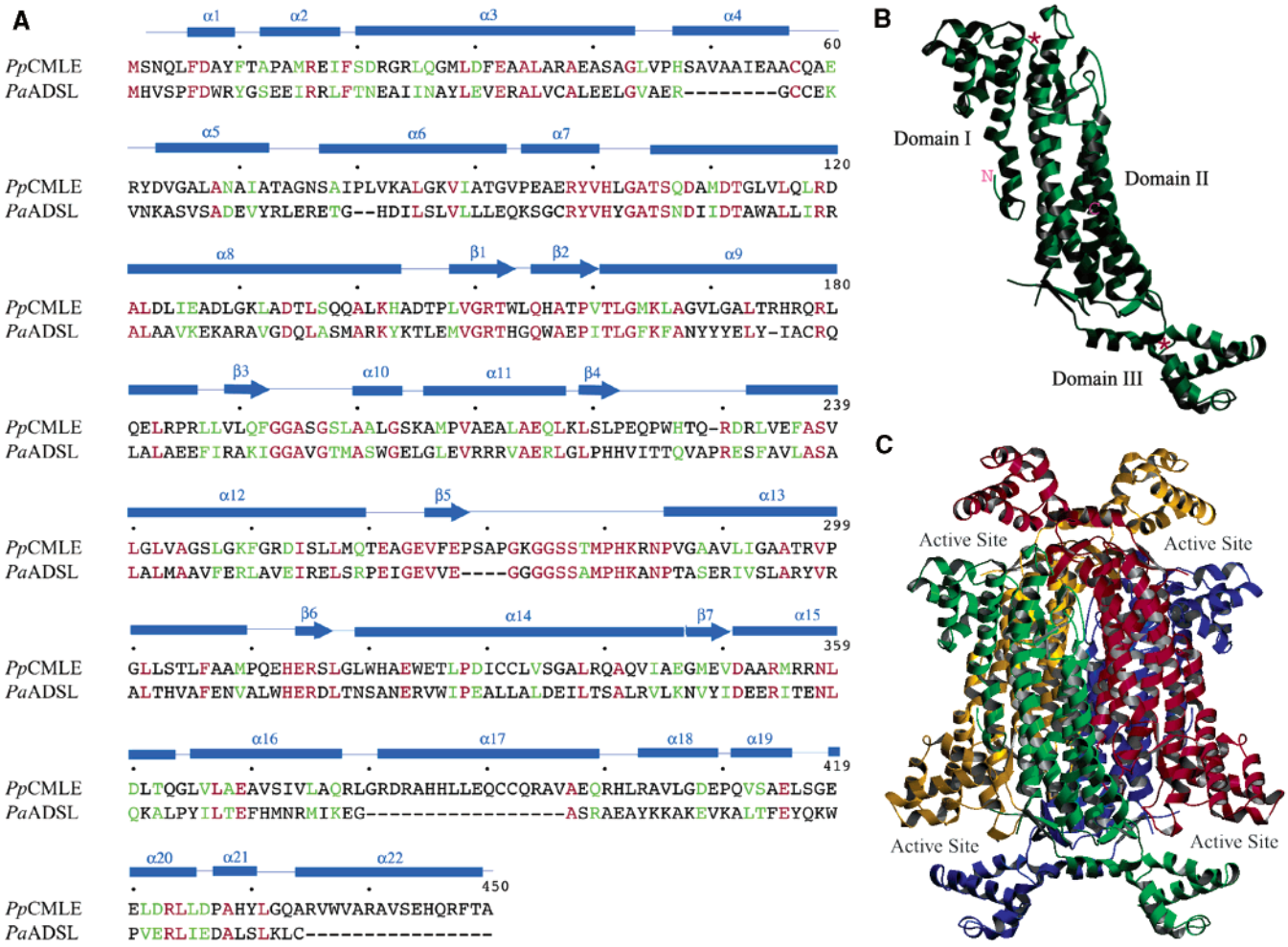

FIGURE 4: Overall structure of *Pp*CMLE. (A) Pairwise amino acid sequence alignment of *Pp*CMLE and *Pa*ADSL with the identical and homologous residues labeled in red and green, respectively. The secondary structure of *Pp*CMLE determined from PROCHECK is also presented with α-helices and *β*-strands shown as rectangles and arrows, respectively. (B) Ribbon representation of the monomeric *Pp*CMLE molecule with the three domains labeled. The N- and C-termini are labeled. The linker regions between domain I and domain II and between domain II and domain III are labeled with red asterisks. (C) Ribbon representation of the tetrameric *Pp*CMLE molecule. Subunits A−D are shown in green, red, blue, and yellow, respectively. The four active site regions are also labeled. This figure was prepared using Molscript (*44*) and Povscript+ (*45*).

evolution of the muconate lactonizing enzymes. Since the muconate lactonizing enzymes are involved in the biodegradation of aromatic compounds and many of these compounds are important pollutants in the environment, our results may also be used as a guideline for structure-based modifications of *Pp*CMLE to achieve faster and cleaner biodegradation of these environmental pollutants. Through the comparison of *Pp*CMLE with MLEs, eukaryotic CMLEs, and other fumarase class II superfamily members, we may also gain a better understanding of the catalytic and regulatory mechanisms of the 1,2-addition−elimination reaction.

EXPERIMENTAL PROCEDURES

Expression and Purification. *Pp*CMLE was expressed and purified using the published protocol in the presence of 5 mM DTT (*3*). The plasmid containing the *Pp*CMLE gene under control of the lac promoter was transformed into *Escherichia coli* strain N4830. A 5 mL culture of *E. coli* N4830 that had been grown for 12 h at 30 °C in LB medium containing 35 μg/mL ampicillin was used to inoculate 1 L of the same medium. The inoculated culture was allowed to grow at 30 °C until the OD of the culture reached 0.6−0.9. Protein expression was then induced with IPTG, and cell growth proceeded for an additional 2 h with the temperature increased to 42 °C. The cells were harvested by centrifugation at 5000*g* for 20 min, and the pellets were stored at −20 °C.

A frozen pellet weighing 1.08 g was resuspended in 20 mL of cold buffer A [0.25 M ethylenediamine dichloride (pH 7.3), 1 mM EDTA, 10 mM DTT, and 5 mM PMSF]. The cells were disrupted by sonication, and the cell lysate was then centrifuged at 10000*g* for 30 min at 4 °C. All subsequent steps were performed at 4 °C. The supernatant was loaded onto a DEAE-Sepharcel column (2.5 cm × 18 cm) that was pre-equilibrated with buffer A. After the mixture had been washed with buffer A until the elute absorbance was less than 0.03, the protein was eluted with a linear NaCl gradient from 0.0 to 0.5 M in buffer A at a flow rate of 1 mL/min. The protein eluted in the range of 0.25−0.40 M NaCl. The purity of *Pp*CMLE in the elution fractions was examined by SDS−PAGE. Fractions containing *Pp*CMLE were pooled, concentrated to 10 mL using an Amicon stir cell with a PM-30 membrane, and buffer-exchanged with buffer B [1 mM NaP_i (pH 7.3) and 10 mM

Table 1: Data and Refinement Statistics

data statistics	
unit cell (Å)	$a = b = 231.52$, $c = 78.46$
space group	$P6_5$
resolution (Å)	2.6
no. of measured reflections	134573
no. of unique reflections	68355
data completeness (%)	92.2 (89.2)[a]
R_{sym} (%)	10.8 (56.2)[a,b]
refinement statistics	
resolution range (Å)	20−2.6
R-factor (%)	21.2 (35.0)[c]
R_{free} (%)	24.2 (35.2)[c,d]
rms differences for bond distances (Å)	0.008
rms differences for bond angles (deg)	1.3
estimated coordinate error (Å)	0.3
average *B*-factor for protein atoms (Å^2)	36.7
Ramachandran analysis	
% favored	90.9
% additional	8.5
% generous	0.6
% disallowed	0.0

[a] Values in parentheses correspond to the highest-resolution shell (2.69−2.60 Å). [b] $R_{sym} = \sum|I_{hkl} - I_{hkl}|/\sum I_{hkl}$, where I_{hkl} is the mean intensity of all reflections equivalent to reflection *hkl* by crystal symmetry. [c] Values in parentheses correspond to the highest-resolution shell (2.62−2.60 Å). *R*-factor (R_{free}) $= \sum||F_o| - |F_c||/\sum|F_o|$, where F_o and F_c are the observed and calculated structure factors, respectively. [d] Ten percent of the diffraction data were randomly selected as a test set for calculation of R_{free}.

DTT]. The protein was then chromatographed on a hydroxylapatite column (2.5 cm × 8 cm). A linear phosphate gradient between 0.1 and 0.5 M was used with a flow rate of 0.33 mL/min. The purity of *Pp*CMLE in the elution fractions was also examined by SDS−PAGE. The fractions containing pure *Pp*CMLE were combined and concentrated to 20 mg/mL. The final protein with an estimated purity of >95% was flash-frozen in liquid nitrogen and stored at −80 °C.

Crystallization and Data Collection. Crystallization of *Pp*CMLE was performed by the hanging-drop vapor-diffusion method at room temperature. Initial crystallization conditions were obtained by the sparse-matrix protocol (*35*). Optimized conditions included equal-volume mixtures of a protein solution [20 mg/mL in 1 mM NaP_i (pH 7.3)] and a reservoir solution [12−18% PEG8000, 5 mM DTT, and 40 mM NaP_i (pH 7.3)] equilibrated against the reservoir solution (1 mL). Crystals with a maximum size of 1.0 mm × 0.7 mm × 0.5 mm were obtained within 1 week. A 2.6 Å resolution diffraction data set was collected from a single crystal mounted in a quartz capillary tube at 4 °C on a Rigaku RAxis IV image plate detector installed on a Rigaku RU300B generator running at 40 kV and 130 mA. The diffraction data were processed with DENZO and SCALEPACK (*36*). Crystals of *Pp*CMLE have the symmetry of hexagonal space group $P6_5$ with the following unit cell parameters: $a = b =$ 231.52 Å, $c = 78.46$ Å, $\alpha = \beta = 90°$, and $\gamma = 120°$. There are four *Pp*CMLE molecules, forming a homotetramer, in the asymmetric unit. The detailed statistics of the diffraction data are summarized in Table 1.

Structure Determination and Refinement. The crystal structure of *Pp*CMLE was determined by the molecular replacement method with CNS (*37*), using atomic coordinates of the tetrameric *Pyrobaculum aerophilum* ADSL (PDB entry 1DOF) as the search model (*24*). At the time, the sequence of this protein was the most similar (37% identical and 45% similar; Figure 4A) to that of *Pp*cMLE. In the search model, all nonidentical residues between *Pp*CMLE and *Pa*ADSL were mutated to alanine residues. The rotation search gave a unique solution, but the top 10 translation solutions were not distinguishable from one another based on the monitor index. Of these, the second solution provided the best crystal packing. Therefore, the second translation solution was selected and subjected to model refinement with CNS using all data in the 20−2.6 Å resolution range. Refinement was done by CNS with a maximum likelihood target function, and monitored by the R_{free} factor (*38*) that was calculated using a randomly selected set of reflections (10% of the data) as the test set. Subsequent model building, which was interspersed with CNS refinement, was done with O (*39*). Noncrystallographic symmetry (NCS) restraints were applied to the four molecules in the asymmetric unit, and NCS restraint weights were reduced to 80 and 30 for the main chain and side chain atoms, respectively, after the 10th cycle of refinement. The residues from Ser269 to Lys282 in conserved but flexible region 3 were not included in the NCS restraints. During the refinement of the model, we observed two regions of strong electron density (>2.5σ) at the center of the tetrameric *Pp*CMLE molecule. Two DTT molecules were modeled into this electron density and included in subsequent refinement cycles. In total, 16 cycles of model refinement and manual building were performed. In the final cycle, the crystallographic *R*-factor and R_{free} equaled 21.2 and 24.2%, respectively. An unidentified electron density feature was observed at the active site formed by subunits B−D in the final difference electron density map with $F_o - F_c$ coefficients. A number of compounds, taken from the known composition of the buffers and crystallization medium that were used, were examined as potential models for this electron density. None fit. In addition, the substrate 3-CM was docked into this electron density with a remarkably good fit. The final model contained four *Pp*CMLE monomers, 100 water molecules, and two DTT molecules. The quality of the final model was examined by PROCHECK (*40*), and the final model had 90.9% of the total amino acid residues in the most favored core region and none in the disallowed region in the Ramachandran plot. The final refinement

Table 2: Buried Surface Areas (Å^2) between Monomers in the *Pp*CMLE Tetramer

	monomer A	monomer B	monomer C	monomer D
monomer A	NA[a]	7365	1854	4154
monomer B	7365	NA[a]	4132	1960
monomer C	1854	4132	NA[a]	7399
monomer D	4154	1960	7399	NA[a]

[a] Not applicable.

statistics are summarized in Table 1. The coordinates of CMLE have been deposited in the Protein Data Bank 1RE5.

RESULTS AND DISCUSSION

Overall Structure. The prokaryotic *Pp*CMLE crystallizes as a homotetramer, consistent with the observation that it is a homotetramer in solution. This result is also consistent with other fumarase class II superfamily members which also exist as tetramers. In the crystal structure, there is one tetramer in the asymmetric unit, with the monomers (Figure 4B) packed in an antiparallel fashion and related by exact 222 symmetry (Figure 4C). The root-mean-square (rms) deviations of Cα atoms between subunits in the tetramer are less than 0.1 Å. The *Pp*CMLE monomeric molecule has an asymmetric appearance, while the tetrameric molecule is more or less globular. Each monomer of the protein contains 450 amino acid residues and is divided into three domains: the N-terminal domain (I), the central domain (II), and C-terminal domain (III). Domain I consists of residues Met1−Ala104. However, the first two residues, Met1 and Ser2, were not observed in the final electron density map. Residue Met1 was missing due to partial post-translational cleavage of the methionine in the host cells, *E. coli* N4830 (*3*), whereas residue Ser2 was disordered in the crystal structure. Domain I consists of seven α-helices forming a cluster. Domain I interacts with domain II mainly through helices α1 and α2. Conserved sequence region 1 is the linker between domain I and domain II. Domain II consists of residues Thr105−Gly364. It consists of eight α-helices and seven short *β*-strands. Most of the short *β*-strands are involved in the formation of the active site and substrate recognition. Conserved sequence regions 2 and 3 are located in domain II. Conserved region 2 is well-ordered and forms a *β*-hairpin. However, conserved region 3 is very flexible and only visible in monomer D when the contour level of an electron density map with $2F_o - F_c$ coefficients is lowered to 0.7σ. Residues from this region, residues Gly272−His281, residues Gly272−Thr278, and residues Ala270−Ser277 in monomer subunits A−C, respectively, are disordered. The five central long α-helices (α8, α9, and α12−α14) in domain II of each monomer come together to form a bundle of 20 α-helices, which makes up the core of the *Pp*CMLE tetrameric molecule. Remarkably similar to the case with fumarase C (*20*, *21*), most of the α-helices in the bundle of 20 α-helices exhibit small amounts of curvature to accommodate tight packing at the interfaces of the monomers. C-Terminal domain III is comprised of residues Leu365−Ala450 and contains seven α-helices. Formation of the homotetrameric molecule buries more than 26 000 Å^2 of surface area with as much as 55% of the surface area contributed by the A−B and C−D interfaces [7365 and 7399 Å^2, respectively (Table 2)]. Both electrostatic interactions and hydrophobic contacts are involved at these interfaces.

Comparison with Other Fumarase Class II Superfamily Members. The fumarase class II superfamily members are characterized structurally by a bundle of 20 α-helices and the unique intersubunit composition of the active site. We superimposed tetrameric domain II of *Pp*CMLE onto those of the other superfamily members (Figure 5A). The rms deviations of Cα atoms between *Pp*CMLE and the other members were less than 1.8 Å (Table 3). However, the orientations of domain I and domain III with regard to domain II are different among members of the superfamily. Nevertheless, both domain I and domain III were more or less confined in a narrow region. This narrow region may be required to guarantee that the active site is properly formed and possesses some flexibility to confer substrate specificity for each respective member. Superposition of the individual domains I revealed that the positions of only three of the seven α-helices (α3, α4, and α6) are conserved (Figure 5B). The rms deviations between domain I of *Pp*CMLE and other members are less than 2.2 Å. We also superimposed domain III among the family members (Figure 5C). Helices α16 and α17 are conserved in all the superfamily members, but helix α22 is conserved in only *Pp*CMLE, *Pa*ADSL, human ARSL, and duck *δ*2-crystallin. The rms deviations for domain III between *Pp*CMLE and the other superfamily members are less than 1.7 Å. On the basis of the superposition studies, *Pa*ADSL and human ARSL are structurally the closest and most distant relatives, respectively, of *Pp*CMLE in the superfamily.

Small Molecular Binding Sites. Two features of electron density are observed in the electron density map for which atoms of the enzyme polypeptide cannot account. One of these, right at the geometric center of the tetrameric *Pp*CMLE molecule, is observed at a level of $>2.5\sigma$ in a difference electron density map with $F_o - F_c$ coefficients (Figure 6A). The shape of each region of electron density strongly suggested that it was a DTT molecule. However, the sulfur anomalous scattering signal was not strong enough to unambiguously confirm the presence of DTT. Since 5 mM DTT was present during protein expression, it may be that DTT molecules were encapsulated during the formation of the *Pp*CMLE homotetramer. Therefore, two DTT molecules were added to the model and subjected to refinement. The average *B*-factor for the two DTT molecules (110 Å^2) was much larger than the average *B*-factor for the protein (36.7 Å^2), suggesting that the two DTT molecules were not at full occupancy. The occupancies for the DTT molecules were not refined due to the limitation of the moderate-resolution diffraction data. The positions of the two DTT molecules were ∼7 Å apart and related by 2-fold symmetry with the symmetry axis running through the center of the *Pp*CMLE tetrameric molecule. Both DTT molecules are oriented perpendicular to the central bundle of 20 α-helices of *Pp*CMLE and interact exclusively with helix α13 of each monomer, largely with residues 296−304 (Figure 6B). Atom S1 of DTT801 is in position to make three putative hydrogen bonding interactions with the main chain N atom of residue Gly300A, the main chain carbonyl O atom of residue Thr296A, and the side chain hydroxyl group of residue Thr304D, while atom S4 makes similar hydrogen bonding interactions with residues Gly300C, Thr296C, and Thr304B. This rare type of encapsulation has not been observed for

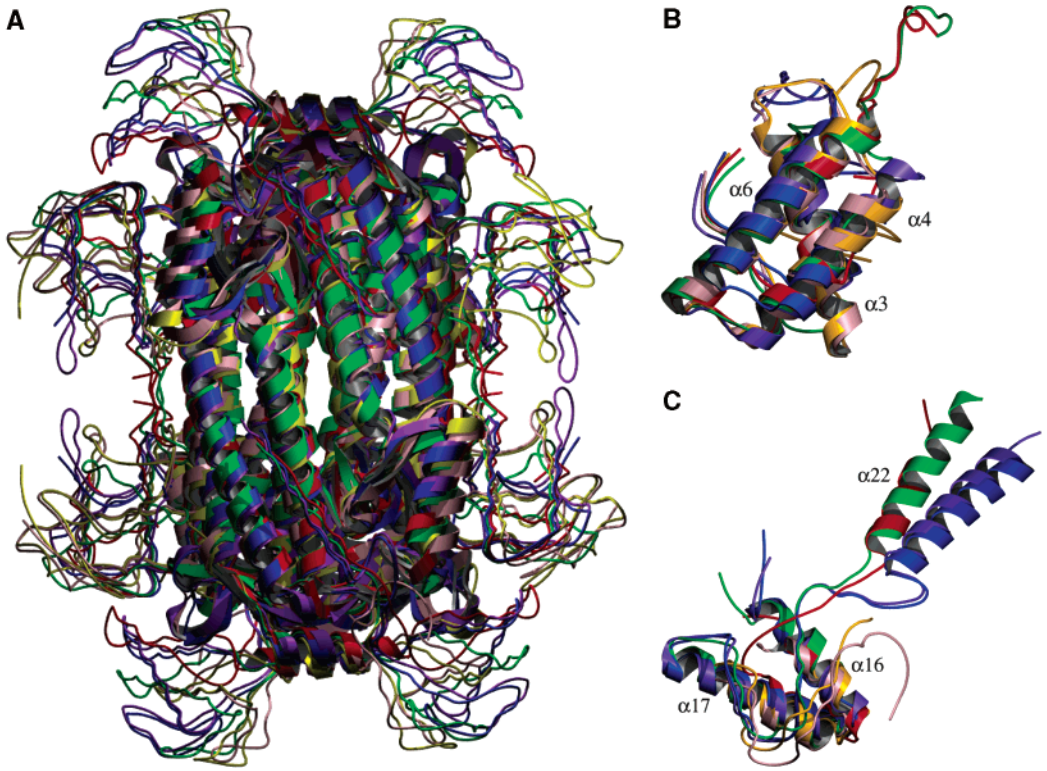

FIGURE 5: Structural superimposition of all of the fumarase class II family members at tetrameric central core domain II (A), monomeric N-terminal domain I (B), and monomeric C-terminal domain III (C). *Pp*CMLE, *Pa*ADSL, yeast fumarase C, hARSL, duck δ2-crystallin, and *Bacillus* sp. YM55-1 aspartase are labeled in green, red, yellow, blue, purple, and pink, respectively.

Table 3: rms Differences (Å) between *Pp*CMLE and Other Fumarase Class II Enzymes

	monomer			tetramer
	domain I	domain II	domain III	domain II
Py. aerophilum ADSL	1.37	1.44	1.76	1.43
yeast fumarase C	1.46	1.56	1.61	1.65
human ARSL	2.20	1.66	1.72	1.82
duck δ2-crystallin	1.49	1.52	1.72	1.79
Bacillus sp. YM55-1 aspartase	1.65	1.60	1.54	1.75

the other members of the fumarase class II superfamily members. It is not clear whether there is any significance to this small molecule binding site.

A second feature of electron density is observed at the putative active site, potentially representing a small molecule, and will be discussed below.

Location of the Active Site. The locations of the active sites for the other fumarase class II superfamily members have been extensively investigated and are located in conserved regions of the oligomer (*20*, *21*, *23*, *24*, *26*, *27*, *30*, *31*, *33*). Consequently, the active sites of *Pp*CMLE are expected to be in similar regions of its overall structure. The active site configuration was explored by comparison with that of fumarase C because this is the only member of the superfamily for which structures of complexes are available, one with citric acid bound and one with pyromellitic acid bound (*20*). The *Pp*CMLE structure was superimposed on the fumarase C−citrate complex structure at the putative active site region (Figure 7). The active sites for the two enzymes superimposed very well, suggesting that *Pp*CMLE and fumarase C recognize the fumarate moiety in their substrates using similar residues. On the basis of this comparison, the tetrameric *Pp*CMLE molecule has four active sites, and each active site is formed predominantly by residues from the three conserved regions donated by three respective monomers (Figure 4C). The active site is situated in a deep pit on the surface that is slightly negatively charged (Figure 8). Domains I and III, which come from two different monomers, act like upper and lower jaws, respectively, to guard the active site.

This study is of the native structure of *Pp*CMLE as no inhibitors or ligands were intentionally added during the protein purification and crystallization. Surprisingly, we identified a strong feature of electron density (>2.5σ) in the final difference electron density map ($F_o - F_c$ coefficients) at the presumed active site formed by monomers B−D. As this electron density was observed at only one of the four active sites, the binding of a molecule at this position is presumed to be weak. Efforts to model this electron density with obvious components of the crystal mother liquor did not provide a convincing identity. The best fit could be obtained for the substrate 3-CM (or an inhibitor analogue), but it is not clear from where such a molecule would be derived. Nevertheless, the position of this feature can be used to indicate the location of the active site and potential interacting residues that could stabilize the binding of the substrate.

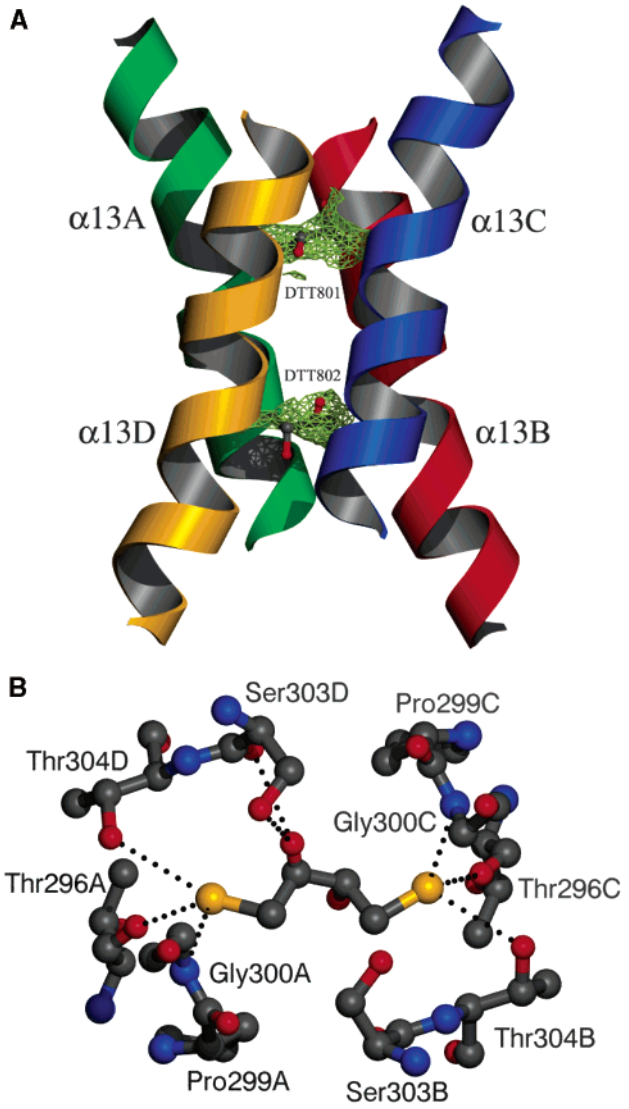

FIGURE 6: Representation of the two DTT molecules (DTT801 and DTT802) identified at the center of the tetrameric *Pp*CMLE structure. (A) Omit electron density map with $F_o - F_c$ coefficients contoured at the two DTT molecules. The contour level is 2.5σ. (B) Detailed interactions between DTT801 and *Pp*CMLE. The dotted lines represent potential hydrogen bonds with distances of <3.5 Å between the donor and acceptor.

The position of this electron density feature and the superposition of *Pp*CMLE with fumarase were used to attempt the identification of the recognition residues for the substrate. In fumarase C, the presence of bound citrate was used to identify potential substrate recognition residues. In the structure of this complex, one carboxylate interacts with residues Lys324 and Asn326 from conserved region 3, Thr187, and Asn141 from conserved region 1 (Figure 7). These residues are equivalent to residues Lys282, Asn284, Thr152, and Gln107, respectively, in *Pp*CMLE. In fumarase, conserved region 3 has been suggested to be a "signature sequence" for enzymes that catalyze β-elimination reactions and generate fumarate as a product (*41*). This interpretation may be partially correct, in that this region could be the one contributing to the recognition of the substrate at the carboxylate closest to the atom at which attack of the oxygen nucleophile occurs. A second carboxylate of the citrate inhibitor bound to fumarase interacts with a number of residues with hydrogen bonding capabilities, but none of these residues is conserved across the superfamily. Since only fumarate and 3-CM have a second carboxylate, a group that is not conserved in many of the substrates recognized by enzymes of the superfamily, one can only speculate that these residues could recognize the second carboxylate of fumarate or, by homology, 3-CM. The third carboxylate of citric acid in the structure of the fumarate complex points toward His188. This residue has been identified as the catalytic base in the fumarase reaction. It is conserved in all of the other superfamily members, except CMLE. The significance of this lack of conservation may be related to the fact that CMLE catalyzes an intramolecular variant of the fumarate reaction.

Structural Comparison with NcCMLE. Because the substrate and type of reaction catalyzed by *Pp*CMLE and *Nc*CMLE are superficially similar, comparisons of the structures of these enzymes could help identify the residues associated with substrate recognition and catalysis. Especially if the reactions catalyzed follow similar pathways, the active sites may have converged and therefore have some similarities. The overall structure of *Pp*CMLE is completely different from that of the eukaryotic *Nc*CMLE. Obvious differences between the two include the location and makeup of the active site, which is located at the interface of three monomers in *Pp*CMLE and completely contained within one monomer in *Nc*CMLE. None of the residues contained in or near the active sites correspond to each other. The active site of *Pp*CMLE is overall slightly negatively charged (Figure 8), indicating that the negatively charged 3-CM might need to overcome an electrostatic barrier to move into the active site, whereas the active site of *Nc*CMLE is positively charged.

In fact, these two enzymes catalyze very different types of reactions, albeit with the same substrate. The *anti*-1,2-addition−elimination reaction catalyzed by *Pp*CMLE involves the attack of the 6-CO_2^{2-} group on C3 of the substrate to form 4-carboxymuconolactone, whereas the *syn*-1,2-addition−elimination reaction catalyzed by *Nc*CMLE involves the attack of the 1-CO_2^{2-} group of 3-CM on C4 to form 3-carboxymuconolactone. In conclusion, in keeping with the fact that the details of the reaction catalyzed by these two enzymes are different, the structures are very different, accommodating different recognition elements and different catalytic steps.

Putative Catalytic Mechanism. Mechanistic studies of the enzyme, sequence comparisons, and now the three-dimensional structure suggest that *Pp*CMLE can be classified as a fumarase class II type enzyme. It is the only one of this family of enzymes that catalyzes an intramolecular variant of the fumarase reaction. The distinguishing feature of this type of reaction is the *anti* addition of a nucleophile and a proton across a double bond (Figure 2). Unfortunately, since there are no inhibitor complexes of members of this family that can uniquely identify the binding mode of a substrate, structural comparison and sequence conservation have been used to indicate the residues that are most likely to be involved in substrate recognition (Figure 7) and catalysis. Most of the residues involved in recognition of the substrate are derived from conserved regions 1 and 3 and have been discussed above. Conserved sequence region 2 contains the residue that acts as a general base in fumarase catalysis, and in the reactions catalyzed by all other members of the

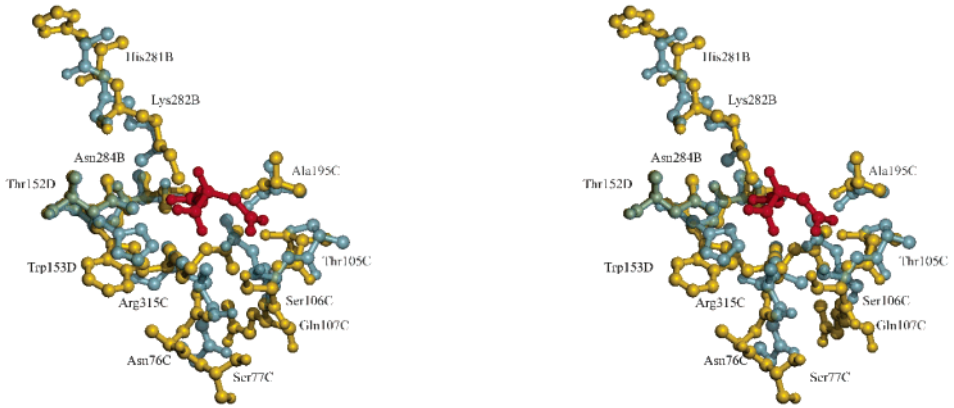

FIGURE 7: Stereo representation of the superimposition of the active sites of *Pp*CMLE and yeast fumarase C. The residues forming the active site from *Pp*CMLE and yeast fumarase C are shown in yellow and light blue, respectively. The citrate molecule bound to the active site of yeast fumarase C is shown in red. Only the *Pp*CMLE active residues are labeled. The residues corresponding to Asn76C, Ser77C, Thr105C, Ser106C, Gln107C, Thr152D, Trp153D, Ala195C, His281B, Lys282B, and Asn284B in *Pp*CMLE are Gly99C, Thr100C, Ser139C, Ser140C, Asn141C, Thr187D, His188D, Ala231C, Gly323B, Lys324B, and Asn326, respectively, in fumarase C.

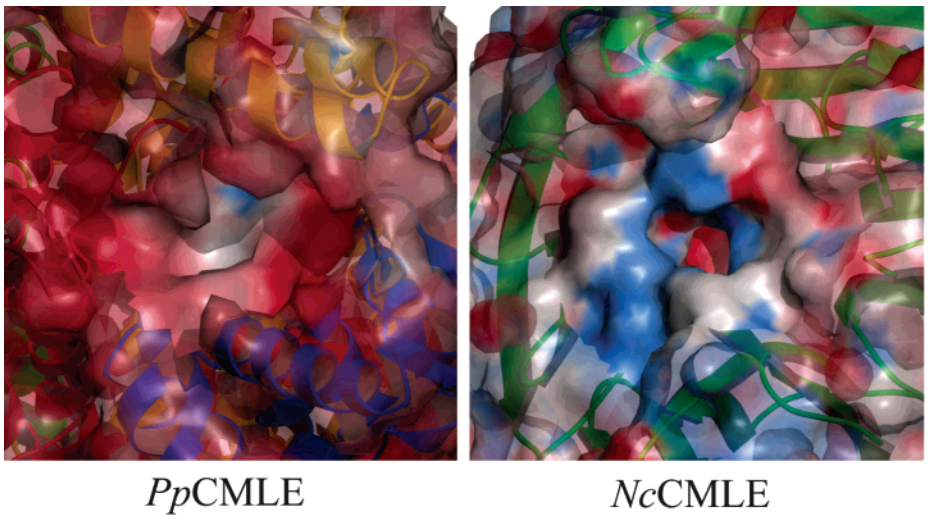

FIGURE 8: Comparison of the electrostatic potential distribution of the active site of *Pp*CMLE and *Nc*CMLE. The electrostatic potential distribution is shown in the same scale [from red (−30) to blue (30) through white (0)] for *Pp*CMLE and *Nc*CMLE. This figure was prepared using GRASP (*46*) and Povscript+ (*45*).

superfamily, with the exception of *Pp*CMLE. In *Pp*CMLE, this residue is a tryptophan (Trp153; see Figures 3 and 7). In the fumarase-catalyzed reaction, this base is required to enhance the reactivity of the attacking nucleophile. The attacking nucleophile is water in the case of fumarase, and therefore, a general base is critical. It is arguable that this base is not required for the *Pp*CMLE reaction because the attacking nucleophile, one of the oxygens of a carboxylate group, is already ionized due to its low pK_a, and therefore does not require catalytic deprotonation to enhance its reactivity. However, a carboxylate is not particularly reactive, suggesting that other ways must be available for the enzyme to accelerate the reaction. One of these is the decreased entropic cost of the reaction due to the fact that the reaction is intramolecular. The other is the influence of the protein environment in the vicinity of the carboxylate group that could enhance its reactivity. The tryptophan in place of a histidine would provide such an environment by enhancing the hydrophobic character of the region, thereby enhancing the reactivity of the attacking carboxylate. It is therefore suggested that this enzyme has uniquely evolved to allow hydrophobic activation for the carboxylate nucleophile. Such activation has been suggested for other enzymes such as thiamine-dependent decarboxylase (*42*) and decarboxylation of orotidine monophosphate decarboxylase (*43*). We have argued that Lys282 could be involved in substrate recognition, based on sequence conservation and comparison with the structure of the fumarase−citrate complex. However, it is also possible that Lys282 can carry out proton delivery. On the basis of the model of 3-CM built into the electron density feature found at one of the active sites of the *Pp*CMLE model, this residue could be in an orientation to act as an acid to give the product. If this orientation is even close to correct, then the aci-carboxylate group of the transition state is in position to be stabilized by Arg315. The electrostatic potential distribution at the active site of *Pp*CMLE (Figure 8) shows that the only small patch of positive potential in the active site is around this residue. Since *Pp*CMLE is the only enzyme for which such stabilization is suggested, this residue would not be expected to be conserved across family members, and it is not.

Comparisons for syn- and anti-Cycloisomerases. Despite catalyzing apparently similar reactions, the *syn*-cycloisom-

erases represented by *Pp*MLE and *Nc*CMLE and the *anti*-cycloisomerases typified by *Pp*CMLE show significant differences in their respective catalytic mechanisms (Figure 2). The first step of the lactonization reaction catalyzed by *Pp*MLE starts with the protonation of the substrate *cis,cis*-muconate at 6-CO_2^{2-} by general acid Glu327, followed by the cyclization to form an enol intermediate. The enol intermediate then undergoes proton transfer from general base Lys169 to the intermediate, followed by proton release from the intermediate back to general acid Glu327 to form the final product muconolactone (*7*). The other representative of the *syn*-cycloisomerase, *Nc*CMLE, catalyzes its reaction using a very similar mechanism (*8*). The lactonization by *Nc*CMLE is also thought to proceed via an enol intermediate. In that enzyme, general acid Glu212 is crucial for enzyme activity, as shown by the mutant Glu212Ala which is almost inactive. A general base is identified as residue His148, which is conserved among related family members. The His148Ala variant is completely inactive. For the *anti*-cycloisomerase *Pp*CMLE, there is no acidic residue in the vicinity of the active site, suggesting that the reaction catalyzed by *Pp*CMLE does not require a general acid or uses a different mechanistic pathway. The requirement for a general base has already been discussed and also suggests a different mechanistic pathway. In summary, by analogy to the reaction catalyzed by fumarase, the lactonizing reaction catalyzed by *Pp*CMLE could also proceed in a stepwise fashion. The first step would be the nucleophilic attack of the oxygen of the 6-CO22- group at position C3, aided by the hydrophobic environment around this group, to form an aci-intermediate stabilized by residue Arg315. The second step would be proton transfer from a general base such as Lys282 to the aci-intermediate to form the observed product. Thus, the *syn*- and *anti*-cycloisomerases have experienced distinct evolutionary pathways to suit their respective recognition and catalytic requirements.

ACKNOWLEDGMENT

We thank Dr. Tim Fenn for his help with the graphics.

REFERENCES

1. Stanier, R. Y., and Ornston, L. N. (1973) The β-ketoadipate pathway, *Adv. Microb. Physiol. 9*, 89−151.
2. Ornston, L. N., and Yeh, W. K. (1982) in *Recruiting themes and repeated sequences in metabolic evolution: biodegradation and detoxification of environmental pollutants* (Chakrabarty, A. M., Ed.) pp 105−126, CRC Press, Boca Raton, FL.
3. Williams, S. E., Woolridge, E. M., Ransom, S. C., Landro, J. A., Babbitt, P. C., and Kozarich, J. W. (1992) 3-Carboxy-*cis,cis*-muconate lactonizing enzyme from *Pseudomonas putida* is homologous to the class II fumarase family: a new reaction in the evolution of a mechanistic motif, *Biochemistry 31*, 9768−9776.
4. Mazur, P., Pieken, W. A., Budihas, S. R., Williams, S. E., Wong, S., and Kozarich, J. W. (1994) Cis,cis-muconate lactonizing enzyme from *Trichosporon cutaneum*: evidence for a novel class of cycloisomerases in eukaryotes, *Biochemistry 33*, 1961−1970.
5. Chari, R. V. J., Whitman, C. P., Kozarich, J. W., Ngai, K. L., and Ornston, L. N. (1987) Absolute stereochemical course of the 3-carboxymuconate cycloisomerases from *Pseudomonas putida* and *Acinetobacter calcoaceticus*: analysis and implications, *J. Am. Chem. Soc. 109*, 5514−5519.
6. Gerlt, J. A., and Gassman, P. G. (1992) Understanding enzyme-catalyzed proton abstraction from carbon acids: details of stepwise mechanisms for β-elimination reactions, *J. Am. Chem. Soc. 114*, 5928−5934.
7. Helin, S., Kahn, P. C., Guha, B. L., Mallows, D. G., and Goldman, A. (1995) The refined X-ray structure of muconate lactonizing enzyme from *Pseudomonas putida* PRS2000 at 1.85 Å resolution, *J. Mol. Biol. 254*, 918−941.
8. Kajander, T., Merckel, M. C., Thompson, A., Deacon, A. M., Mazur, P., Kozarich, J. W., and Goldman, A. (2002) The structure of *Neurospora crassa* 3-carboxy-*cis,cis*-muconate lactonizing enzyme, a β propeller cycloisomerase, *Structure 10*, 483−492.
9. Babbitt, P. C., Hasson, M. S., Wedekind, J. E., Palmer, D. R. J., Barrett, W. C., Reed, G. H., Rayment, I., Ringe, D., Kenyon, G. L., and Gerlt, J. A. (1996) The enolase superfamily: a general strategy for enzyme-catalyzed abstraction of the α-protons of carboxylic acids, *Biochemistry 35*, 16489−16501.
10. Goldman, A., Ollis, D. L., and Steitz, T. A. (1987) Crystal structure of muconate lactonizing enzyme at 3 Å resolution, *J. Mol. Biol. 194*, 143−153.
11. Hasson, M. S., Schlichting, I., Moulai, J., Taylor, K., Barrett, W., Kenyon, G. L., Babbitt, P. C., Gerlt, J. A., Petsko, G. A., and Ringe, D. (1998) Evolution of an enzyme active site: the structure of a new crystal form of muconate lactonizing enzyme compared with mandelate racemase and enolase, *Proc. Natl. Acad. Sci. U.S.A. 95*, 10396−10401.
12. Neidhart, D. J., Kenyon, G. L., Gerlt, J. A., and Petsko, G. A. (1990) Mandelate racemase and muconate lactonizing enzyme are mechanistically distinct and structurally homologous, *Nature 347*, 692−694.
13. Wieczorek, S. J., Kalivoda, K. A., Clifton, J. G., Ringe, D., Petsko, G. A., and Gerlt, J. A. (1999) Evolution of enzymatic activities in the enolase superfamily: Identification of a "new" general acid catalyst in the active site of D-galactonate dehydratase from *Escherichia coli*, *J. Am. Chem. Soc. 121*, 4540−4541.
14. Copley, S. D. (2000) Evolution of a metabolic pathway for degradation of a toxic xenobiotic: the patchwork approach, *Trends Biochem. Sci. 25*, 261−265.
15. Bonanno, J. B., Edo, C., Eswar, N., Pieper, U., Romanowski, M. J., Ilyin, V., Gerchman, S. F., Kycia, H., Studier, F. W., Sali, A., and Burley, S. K. (2001) Structural genomics of enzymes involved in sterol/isoprenoid biosynthesis, *Proc. Natl. Acad. Sci. U.S.A. 98*, 12896−12901.
16. Burley, S. K., and Bonanno, J. B. (2002) Structural genomics of proteins from conserved biochemical pathways and processes, *Curr. Opin. Struct. Biol. 12*, 383−391.
17. Pilloff, D., Dabovic, K., Romanowski, M. J., Bonanno, J. B., Doherty, M., Burley, S. K., and Leyh, T. S. (2003) The kinetic mechanism of phosphomevalonate kinase, *J. Biol. Chem. 278*, 4510−4515.
18. Ainsworth, A. T., and Kirby, G. W. (1968) Stereochemistry of β-carboxy- and β-hydroxymethyl-muconic derivatives, *J. Chem. Soc. C*, 1483−1487.
19. Woods, S. A., Schwartzbach, S. D., and Guest, J. R. (1998) Two biochemically distinct classes of fumarase in *Escherichia coli*, *Biochim. Biophys. Acta 954*, 14−26.
20. Weaver, T., and Banaszak, L. (1996) Crystallographic studies of the catalytic and a second site in fumarase C from *Escherichia coli*, *Biochemistry 35*, 13955−13965.
21. Weaver, T., Lees, M., and Banaszak, L. (1997) Mutations of fumarase that distinguish between the active site and a nearby dicarboxylic acid binding site, *Protein Sci. 6*, 834−842.
22. Stone, R. L., Zalkin, H., and Dixon, J. E. (1993) Expression, purification, and kinetic characterization of recombinant human adenylosuccinate lyase, *J. Biol. Chem. 268*, 19710−19716.
23. Toth, E. A., and Yeates, T. O. (2000) The structure of adenylosuccinate lyase, an enzyme with dual activity in the de novo purine biosynthetic pathway, *Structure 8*, 163−174.
24. Toth, E. A., Worby, C., Dixon, J. E., Goedken, E. R., Marqusee, S., and Yeates, T. O. (2000) The crystal structure of adenylosuccinate lyase from *Pyrobaculum aerophilum* reveals an intracellular protein with three disulfide bonds, *J. Mol. Biol. 301*, 433−450.
25. Piatigorsky, J., O'Brien, W. E., Norman, B. L., Kalumuck, K., Wistow, G. J., Borras, T., Nickerson, J. M., and Wawrousek, E. F. (1988) Gene sharing by δ-crystallin and argininosuccinate lyase. *Proc. Natl. Acad. Sci. U.S.A. 85*, 3479−3483.
26. Turner, M. A., Simpson, A., McInnes, R. R., and Howell, P. L. (1997) Human argininosuccinate lyase: a structural basis for intragenic complementation, *Proc. Natl. Acad. Sci. U.S.A. 94*, 9063−9068.
27. Sampaleanu, L. M., Vallee, F., Thompson, G. D., and Howell, P. L. (2001) Three-dimensional structure of the argininosuccinate

lyase frequently complementing allele Q286R, *Biochemistry 40*, 15570−15580.
28. Piatigorsky, J. (1989) Lens crystallins and their genes: diversity and tissue-specific expression, *FASEB J. 3*, 1933−1940.
29. Piatigorsky, J., Kantorow, M., Gopal-Srivastava, R., and Tomarev, S. I. (1994) Recruitment of enzymes and stress proteins as lens crystallins, *EXS 71*, 241−250.
30. Abu-Abed, M., Turner, M. A., Vallee, F., Simpson, A., Slingsby, C., and Howell, P. L. (1997) Structural comparison of the enzymatically active and inactive forms of δ crystallin and the role of histidine 91, *Biochemistry 36*, 14012−14022.
31. Sampaleanu, L. M., Vallee, F., Slingsby, C., and Howell, P. L. (2001) Structural studies of duck δ1 and δ2 crystallin suggest conformational changes occur during catalysis, *Biochemistry 40*, 2732−2742.
32. Woods, S. A., Miles, J. S., Roberts, R. E., and Guest, J. R. (1986) Structural and functional relationships between fumarase and aspartase. Nucleotide sequences of the fumarase (fumC) and aspartase (aspA) genes of *Escherichia coli* K12, *Biochem. J. 237*, 547−557.
33. Fujii, T., Sakai, H., Kawata, Y., and Hata, Y. (2003) Crystal structure of thermostable aspartase from *Bacillus sp.* YM55-1: structure-based exploration of functional sites in the aspartase family, *J. Mol. Biol. 328*, 635−654.
34. Weaver, T. M., Levitt, D. G., Donnelly, M. I., Wilkens-Stevens, P. P., and Banaszak, L. J. (1995) The multisubunit active site of fumarase C from *Escherichia coli*, *Nat. Struct. Biol. 2*, 654−662.
35. Jancarik, J., and Kim, S. H. (1991) Sparse-matrix sampling: a screening method for crystallization of proteins, *J. Appl. Crystallogr. 24*, 409−411.
36. Otwinowski, Z., and Minor, W. (1997) Processing of X-ray diffraction data collected in oscillation mode, *Methods Enzymol. 276*, 307−326.
37. Brünger, A. T., Adams, P. D., Clore, G. M., DeLano, W. L., Gros, P., Grosse-Kunstleve, R. W., Jiang, J. S., Kuszewski, J., Nilges, M., Pannu, N. S., Read, R. J., Rice, L. M., Simonson, T., and Warren, G. L. (1998) Crystallography & NMR system: A new software suite for macromolecular structure determination, *Acta Crystallogr. D54*, 905−921.
38. Brünger, A. T. (1992) Free *R*-value: a novel statistical quantity for assessing the accuracy of crystal-structures, *Nature 55*, 472−475.
39. Jones, T. A., Zou, J. Y., Cowan, S. W., and Kjeldgaard, M. (1991) Improved methods for building protein models in electron-density maps and the location of errors in these models, *Acta Crystallogr. A47*, 110−119.
40. Laskowski, R. A., MacArthur, M. W., Moss, D. S., and Thornton, J. M. (1993) PROCHECK: a program to check the stereochemical quality of protein structures, *J. Appl. Crystallogr. 26*, 283−291.
41. Aimi, J., Badylak, J., Williams, J., Chen, Z. D., Zalkin, H., and Dixon, J. E. (1990) Cloning of a cDNA encoding adenylosuccinate lyase by functional complementation in *Escherichia coli*, *J. Biol. Chem. 265*, 9011−9014.
42. Crosby, J., and Lienhard, G. E. (1970) Mechanisms of thiamine-catalyzed reactions: a kinetic analysis of decarboxylation of pyruvate by 3,4-dimethylthiazolium ion in water and ethanol, *J. Am. Chem. Soc. 92*, 5707−5716.
43. Wu, N., Mo, Y., Gao, J., and Pai, E. F. (2000) Electrostatic stress in catalysis: structure and mechanism of the enzyme orotidine monophosphate decarboxylase, *Proc. Natl. Acad. Sci. U.S.A. 97*, 2017−2022.
44. Kraulis, P. J. (1991) Molscript: a program to produce both detailed and schematic plots of protein structures, *J. Appl. Crystallogr. 24*, 946−950.
45. Fenn, T. D., Ringe, D., and Petsko, G. A. (2003) POVScript+: a program for model and data visualization using persistence of vision ray-tracing, *J. Appl. Crystallogr. 36*, 944−947.
46. Nicholls, A., Sharp, K., and Honig, B. (1991) Protein folding and association: insights from the interfacial and thermodynamic properties of hydrocarbons, *Proteins 11*, 281−296.

BI036205C